Physical-layer network coding in coherent optical OFDM systems

Xun Guan[1,] and Chun-Kit Chan[1*]

[1]*Department of Information Engineering, The Chinese University of Hong Kong, Hong Kong*
[*]*ckchan@ie.cuhk.edu.hk*

Abstract: We present the first experimental demonstration and characterization of the application of optical physical-layer network coding in coherent optical OFDM systems. It combines two optical OFDM frames to share the same link so as to enhance system throughput, while individual OFDM frames can be recovered with digital signal processing at the destined node.

OCIS codes: (060.4255) Networks, multicast; (060.1660) Coherent communications; (060.2330) Fiber optics communications.

References and links

1. S. Y. R. Li, R. W. Yeung, and N. Cai, "Linear network coding", IEEE Trans. on Info, Theory **49**(2), 371–387 (2003).
2. S. Zhang, S. C. Liew, and P. P. K. Lam, "Physical-layer network coding", presented at *International Conference on Mobile Computing and Networking* (MobiComm), Los Angeles, CA USA (2006), Paper C.2.1.
3. Y. An, F. Da Ros, and C. Peucheret, "All-optical network coding for DPSK signals," presented at *Optical Fiber Communication Conference* (OFC), Anaheim, CA USA (2013), Paper JW2A.60.
4. Z. X. Liu, M. Li, L. Lu, C. K. Chan, S. C. Liew, and L. K. Chen, "Optical physical-layer network coding," IEEE Photon. Technol. Lett. **24**(16), 1424–1427 (2012).
5. Z. Liu, L. Lu, L. You, C. K. Chan, and S. C. Liew, "Optical physical-layer network coding for fiber-wireless," presented at *European Conference on Optical Communications* (ECOC), London, UK (2013), Paper Mo.3.F.3.
6. M. Li, Y. Wu, L. K. Chen, and S. C. Liew, "Common-channel optical physical-layer network coding," IEEE Photon. Technol. Lett. **26**(13), 1340–1342 (2014).
7. W. Shieh, H. Bao, and Y. Tang, "Coherent optical OFDM: theory and design," Opt. Express **16**(2), 841–859 (2008).
8. X. Yi, W. Shieh, and Y. Tang, "Phase estimation for coherent optical OFDM," IEEE Photon. Technol. Lett. **19**(12), 919–921 (2007).

1. Introduction

With the drastic growth in network traffic, spectrum efficient communication technique is highly desirable. Orthogonal frequency division multiplexing (OFDM) technique has been widely recognized as a promising approach to support high-speed optical fiber transmission, owing to its high and flexible spectrum efficiency in both optical and electronic domains, as well as the robustness in combating chromatic dispersion (CD) and polarization mode dispersion (PMD) in optical fiber. In order to enhance the network throughput under limited bandwidth resource, network coding [1], as well as its derivative of physical-layer network coding [2], have emerged as the effective approaches. They have been widely studied in both information theory and wireless communications areas. In optical communications, it is quite challenging to employ network coding, as sophisticated all-optical nonlinear signal processing may be needed at the network nodes [3]. Nevertheless, in order to improve the practicality of network coding in optical networks, we propose to perform optical physical-layer network coding (OPNC) in which the two input optical signals are simply optically combined at the intermediate network node so as to share the same output fiber link for throughput enhancement, and let the destined nodes do the signal separation and recovery process, via electronic digital processing algorithms. The feasibility of this approach has been confirmed by the previously reported works on applying OPNC to optical data frames in on-off keying format [4], as well as in direct-detection OFDM format [5]. Both of these schemes were in direct detection systems, thus the source optical signals had to be set in orthogonal

#234700 - $15.00 USD Received 13 Feb 2015; revised 20 Mar 2015; accepted 29 Mar 2015; published 10 Apr 2015

polarizations. In [6], the application of OPNC in common-channel coherent optical systems, in which the optical signals from different sources were in the same wavelength in polarization-multiplexed differential quadrature phase shift keying (PM-DQPSK) format, was reported. With coherent detection, the signal's polarization constraint was alleviated. In this paper, we further investigate and demonstrate the application of OPNC in a coherent optical OFDM (CO-OFDM) system, for the first time. The results show that the two optically combined CO-OFDM frames could be effectively separated and recovered by electronic digital processing techniques at the destined node. Both common phase errors, as well as carrier frequency offset can be effectively compensated by simple pilot-subcarrier-aided approaches.

The rest of the paper is organized as follows. Section 2 illustrates the basic OPNC in an optical multicast topology and the design considerations of the digital signal processing for the CO-OFDM frames under OPNC. Section 3 presents the experimental demonstration, as well as the numerical simulation results for system characterization. Finally, Section 4 summarizes the paper.

2. Principle of operation

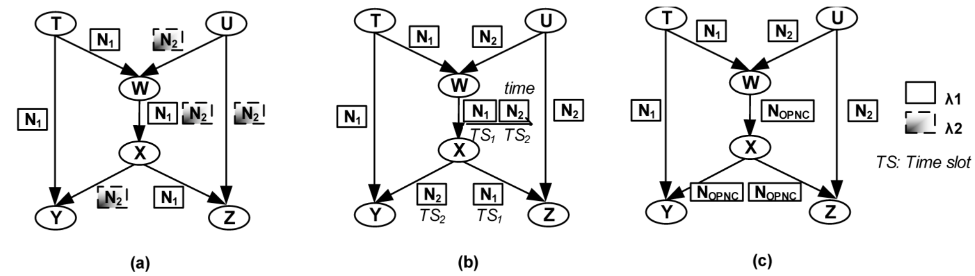

Fig. 1. Optical multicast topology: (a) wavelength division multiplexing, (b) timing division multiplexing, (c) OPNC

The basic principle of OPNC can be illustrated by considering an optical multicast topology, as shown in Fig. 1. Suppose nodes T and U are sending multicast data frames to nodes Y and Z, simultaneously, N_1 is a multicast data frame from node T to nodes Y and Z, while N_2 is another multicast data frame sent from node U to nodes Y and Z. It is assumed that there exists a common link, say W-X, in the network topology. Figure 1(a) illustrates a solution in which N_1 and N_2 are occupying two wavelengths to avoid collisions. Figure 1(b), on the other hand, depicts the case that time division multiplexing is employed to resolve the link contention of the two multicast frames at the expense of requiring two transmission time slots to complete their transmissions. One better approach to save the spectrum or timing resources is to transmit a coded frame, containing the mutual information of N_1 and N_2, on the common link W-X, and each of them are decoded individually at their respective destined nodes, as shown in Fig. 1(c). N_1 and N_2 from nodes T and U are combined at node W to generate a composite OPNC frame, N_{OPNC}, before it is transmitted to nodes Y and Z, via link W-X. In our scheme, the coding at node W is just a simple optical power addition operation. The scheme is limited to combine two source data frames only.

Figure 2(a) depicts a simplified model of CO-OFDM [7]. The orthogonal subcarriers are generated by inverse fast Fourier transform (IFFT) manipulations by digital signal processing (DSP) at the transmitter and the receiver. Ignoring other effects such as laser phase noise and white Gaussian noise, for the simplicity of discussion, one symbol of the transmitted signal in the time domain at point A can be written as

$$x_A(t) = \exp(j2\pi f_{tx}t) \cdot s(t) \qquad (1)$$

#234700 - $15.00 USD Received 13 Feb 2015; revised 20 Mar 2015; accepted 29 Mar 2015; published 10 Apr 2015

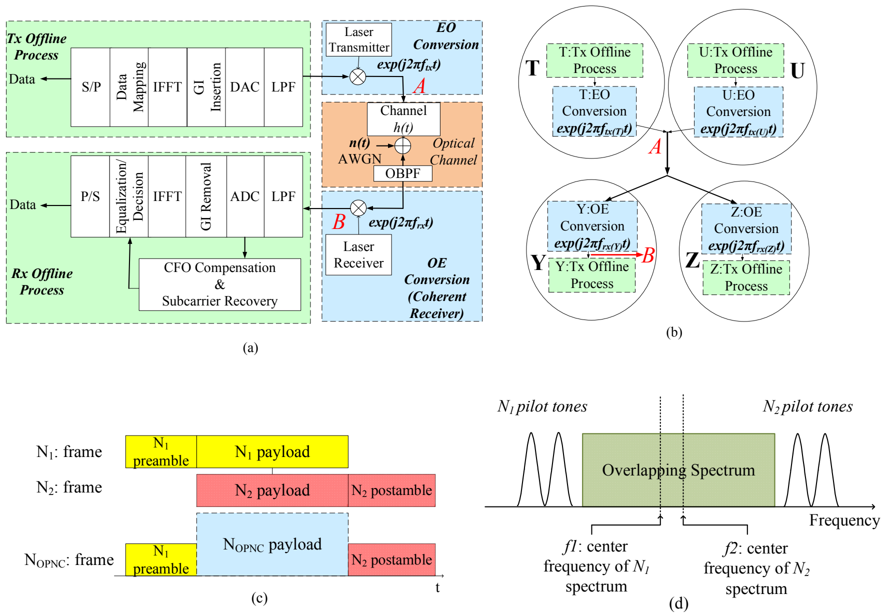

Fig. 2. (a) OFDM model, (b) OPNC model, (c) OPNC frame alignment, (d) OPNC spectrum

$$s(t) = \sum_{k=0}^{N-1} S(k) \cdot \exp(j2\pi f_k t + \theta) = F^{-1}\{S(k)\} \tag{2}$$

$$\Delta f = f_k - f_{k-1}, \quad k-1, k \in [0, N-1] \tag{3}$$

Here, f_{tx} stands for the frequency of the transmitter laser. F^{-1} stands for the inverse Fourier transform. $S(k)$ and f_k are the information symbol and the relative subcarrier frequency at the k^{th} subcarrier, respectively. $s(t)$ is the baseband signal in the time domain. Δf is the subcarrier frequency spacing. θ is the constant phase term within one symbol. The optical signal then passes through the optical channel before being mixed with a local oscillator with frequency f_{rx} at the heterodyne coherent receiver. The signal at point B in Fig. 2(a) can be expressed as

$$x_B(t) = \exp(j2\pi f_{IF} t + \theta) \cdot F^{-1}\{S(k) \cdot H(k)\} \tag{4}$$

$H(k)$ stands for the channel response of the k^{th} subcarrier. f_{IF} is the intermediate frequency f_{IF} determined by the frequency difference between f_{tx} and f_{rx}, that is, $f_{IF} = f_{rx} - f_{tx}$. This component is treated as carrier frequency offset (CFO), which is estimated and compensated by offline DSP at the receiver.

Figure 2(b) shows the model of OPNC corresponding to the topology in Fig. 1. Only the OPNC stream at point Y is depicted. N_1 is sent by T and N_2 is from U. The signal at point A can be written as

$$x_A(t) = \exp(j2\pi f_{tx(T)} t + \theta_1) \cdot s_{N_1}(t) + \exp(j2\pi f_{tx(U)} t + \theta_2) \cdot s_{N_2}(t) \tag{5}$$

$$s_{N_1}(t) = F^{-1}\{S_{N_1}(k)\} \tag{6}$$

$$s_{N_2}(t) = F^{-1}\{S_{N_2}(k)\} \tag{7}$$

where $S_{N1}(k)$ and $S_{N2}(k)$ are the information symbols from T and U, respectively. $s_{N1}(t)$ and $s_{N1}(t)$ are their respective baseband signals in the time domain. The OPNC signal at point B becomes:

#234700 - $15.00 USD Received 13 Feb 2015; revised 20 Mar 2015; accepted 29 Mar 2015; published 10 Apr 2015

$$x_B(t) = \exp(j2\pi f_{IF(N_1)}t + \theta_{N_1}) \cdot F^{-1}\{S_{N_1}(k) \cdot H_{N_1}(k)\} + \exp(j2\pi f_{IF(N_2)}t + \theta_{N_2}) \cdot F^{-1}\{S_{N_2}(k) \cdot H_{N_2}(k)\} \tag{8}$$

Here, $f_{IF(N1)} = f_{rx(Y)} - f_{tx(T)}$, $f_{IF(N2)} = f_{rx(Y)} - f_{tx(U)}$, $H_{N1}(k)$ and $H_{N2}(k)$ stands for the channel response of the k^{th} subcarrier of N_1 and N_2 in the coded signal N_{OPNC}. Assume the information symbols from T has been successfully demodulated and decoded at node Y, which is $S_{N1}(k)$ in this case. To retrieve $S_{N2}(k)$, the channel responses $H_{N1}(k)$ and $H_{N2}(k)$ and the carrier frequency offsets $f_{IF(N1)}$ and $f_{IF(N2)}$ are estimated by inserting training symbols into the OPNC frames. Figure 2(c) depicts the original and the OPNC frames in time domain. In the OPNC frame N_{OPNC}, the non-overlapping symbols are the preamble of N_1 and the postamble of N_2, which will be used for respective carrier frequency offset estimation and channel estimation. Then

$$x_{N_1}(t) = \exp(j2\pi f_{IF(N_1)}t + \theta_{N_1}) \cdot F^{-1}\{S_{N_1}(k) \cdot H_{N_1}(k)\} \tag{9}$$

$$x_{N_2}(t) = x_B(t) - x_{N_1}(t) \tag{10}$$

$$x_{N_2}(t) = \exp(j2\pi f_{IF(N_2)}t + \theta_{N_2}) \cdot F^{-1}\{S_{N_2}(k) \cdot H_{N_2}(k)\} \tag{11}$$

$$S_{N_2}(k) = \frac{F\{x_{N_2}(t) \cdot \exp(-j2\pi f_{IF(N_2)}t - \theta_{N_2})\}}{H_{N_2}(k)}, \quad k = 0, \ldots, N-1 \tag{12}$$

where F stands for the Fourier transform. Once the channel responses and the CFOs have been estimated, $S_{N2}(k)$ can be recovered by fast Fourier transform (FFT), together with an one-tap equalizer in offline DSP. In order to ensure the training symbols in one frame (say N_1) is not overlapping with the payload field of the other frame (say N_2), proper synchronization between the two frames have to be performed, via proper scheduling at their source nodes or proper placement of training symbols in the preambles or postambles of the two frames.

Another major consideration raised in Eq. (9)-(12) is θ_{N1} and θ_{N2}, which are the common phase error (CPE) mainly caused by the phase noise of the laser and this leads to possible rotation in the CO-OFDM information symbols' constellation. Different from CFO and channel response, CPE should be estimated symbol by symbol. In CO-OFDM, pilot tones are inserted to estimate CPE's angle θ based on the fact that CPE is constant over all the subcarriers [7]. However, this effect is even aggravated in the OPNC scenario. In an OPNC symbol N_{OPNC}, the frequency components of the two source OFDM symbols (N_1 and N_2) overlap with each other and they are not guaranteed to be orthogonal to each other. This makes the intra-symbol CPE of the OFDM symbols difficult to be estimated, especially considering that the two CPE's θ_1 and θ_2 should be estimated, simultaneously. However, since it is possible to coarsely control the laser frequency, we can specifically assign the pilot tones at the designated subcarrier frequencies. Figure 2(d) shows the spectrum of an OPNC symbol N_{OPNC}. The center frequency of N_1's spectrum, f_1, and that of N_2's spectrum, f_2, are decided by the local oscillator's (LO) laser frequency, $f_{rx(Y)}$, and the two signal's laser carrier frequencies, $f_{tx(T)}$ and $f_{tx(U)}$. We set the three laser frequencies such that $f_{tx(T)}$ is smaller than $f_{tx(U)}$ by Δf_{tx}, and thus we can insert pilot tones at the lower spectral edge of N_1's spectrum, as well as the upper spectral edge of N_2's spectrum. Suppose the number of non-overlapped pilot subcarriers in two spectra is m, which is indicated by the subcarrier indices as $k = 0$ to $m-1$ of N_1 and $k_2 = (N-m)$ to $(N-1)$ of N_2 in Eq. (6) and (7). The non-overlapping relationship can be guaranteed by

$$\Delta f_{tx} = \left| f_{tx(T)} - f_{tx(U)} \right| \tag{13}$$

$$\Delta f_{tx} \geq m\Delta f \tag{14}$$

#234700 - $15.00 USD Received 13 Feb 2015; revised 20 Mar 2015; accepted 29 Mar 2015; published 10 Apr 2015

Hence, it is possible to estimate the CPE of the N_1 component in N_{OPNC} (CPE_{N1} for $k = 0$ to $(m-1)$), as well as that of the N_2 component in N_{OPNC} (CPE_{N2} for $k = (N-m)$ to $(N-1)$). Note from Eq. (13) that the frequency relationship between $f_{tx(T)}$ and $f_{tx(U)}$ can also be reversed. These estimations can indicate the CPE of the overlapped data subcarriers of their symbols, since CPE is identical over all the subcarriers. The insertion of non-overlapping pilot tones enables the estimation of the respective CPE of the two source optical OFDM signals.

3. Experiments and simulations

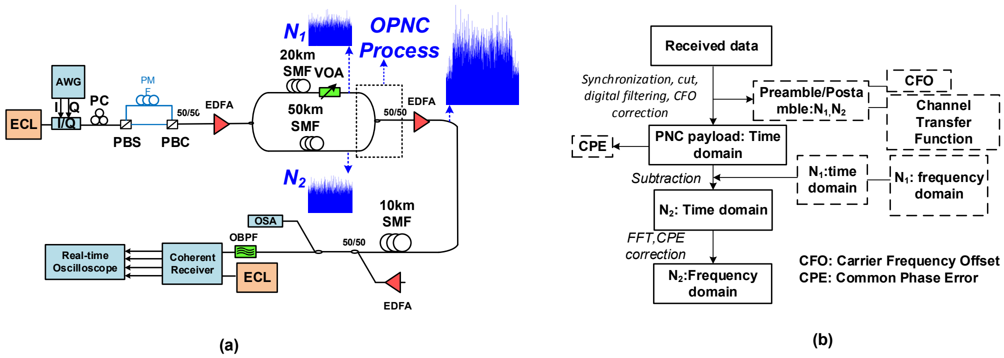

Fig. 3. (a) Experimental setup. AWG: arbitrary waveform generator, ECL: external cavity laser, VOA: variable optical attenuator, OSA: optical spectrum analyzer, OBPF: optical bandpass filter, PC: polarization controller, (b) DSP process

Figure 3(a) depicts the experimental setup. The output of an external cavity laser (ECL) was split into two parts, one of which was adopted as the local oscillator of the coherent receiver. The other laser output was modulated by an optical IQ modulator, driven by the electrical signal from a Tektronix arbitrary waveform generator (AWG), operating at 10 Gsample/s. The offline generated OFDM samples were in FFT size of 256, of which 192 subcarriers were used as data subcarriers and 8 for pilot tones for satisfactory performance [8]. With polarization division multiplexing, the transmission baud rate of this system was 7.5 GBaud. A cyclic prefix (CP) of 8 samples was added. The output of the optical IQ modulator was then divided into two arms, the signal emulating N_1 was transmitted over a separate piece of 20-km single mode fiber (SMF), while the SMF emulating N_2 was 50 km in length. The path difference of 30 km was sufficient to reduce the coherency of the two signals and thus they were used to emulate two optical signals from two different optical sources. Each of these two optical signals was then amplified by its Erbium doped fiber amplifier (EDFA), before being polarization-controlled, via a polarization controller (PC), so as to keep the signal in one polarization state at the receiver. The signal power values of the two arms were controlled to be the same, via an optical variable attenuator (VOA) in one arm, so as to assure optimal operation performance and to facilitate evaluation of the penalty of the OPNC. After combining the output from the two arms, the composite OPNC signal was sent over 20-km SMF. Another EDFA was inserted to control the optical signal-to-noise ratio (OSNR). A portion of the OPNC signal was then fed into an optical spectrum analyzer (OSA) to monitor the OSNR, while the rest was fed into a dual-polarization coherent receiver for detection. An optical bandpass filter (OBPF) with 0.88-nm bandwidth was inserted before the coherent receiver to filter out the out-of-band amplified spontaneous emission noise (ASE), since the coherent receiver was vulnerable to high power. The detected signal was sampled by a Tektronix real-time digital sampling analyzer (DSA). The three insets in Fig. 3 showed the received electrical intensity waveforms after coherent detection of the outputs from the two individual arms, as well as the OPNC signal after transmission, respectively. The received data was decoded by offline digital signal processing (DSP) procedures, which were illustrated in Fig. 3(b).

#234700 - $15.00 USD Received 13 Feb 2015; revised 20 Mar 2015; accepted 29 Mar 2015; published 10 Apr 2015

Figure 4 depicts the comparisons of the cases with and without OPNC in terms of the measured bit-error-rate (BER) of the OFDM frames versus their respective OSNR. The BER was calculated by counting the number of errors over 50 OFDM frames, each of which consisted of 4 training symbols for CFO estimation, 20 training symbols for channel estimation and 400 data symbols. In particular, each OFDM data symbol consisted of 192 quadrature phase shift keying (QPSK) data samples. The actual transmission bit rate was 27.4 Gbit/s. It could be noticed that, at the BER around 10^{-3}, both of the OSNR penalties of OPNC at both arms were about 2 dB, which showed good feasibility of the OPNC decoding.

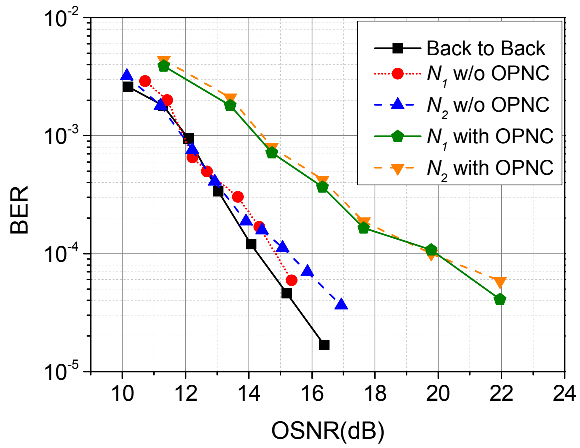

Fig. 4. Measured BER versus OSNR with and without OPNC

The reconstruction of one of the component signals was the key procedure in this scheme. Exact symbol alignment between the two signals is not necessary during the encoding and decoding process, which means that the system performance did not rely on the relative time shift between the two source signals. We have conducted numerical simulation in MATLAB to study BER performance under the influence of the relative time shift (in number of samples) between the two signals, and the results were depicted in Fig. 5(a). It could be noticed that the timing misalignment between the two signals brought slight performance degradation to the decoded signal. Therefore, no stringent sample-level alignment between two code sources was mandatory in OPNC. This feature could largely relieve the constraint of the proposed scheme, and enhance its application in practical scenarios. In addition, the synchronization constraint of the OFDM signal was relieved by the insertion of CP. However, the system performance was actually affected by the synchronization error of the reconstructed signal, since possible imperfect reconstruction produced unintended samples acting as noise in the decoding and demodulation of the decoded signal. Another numerical simulation was also conducted to study the effect of synchronization errors, and the results were depicted in Fig. 5(b). It could be seen that a slight synchronization error, such as one sample, did not bring great influence to the system performance. When the synchronization error continued to increase, the performance started to degrade. Practically, the adoption of advanced synchronization methods could assure the synchronization error of the reconstructed signal in a moderate range, thus the system performance could be guaranteed. Besides, appropriate labels can be added to the header of the optical frames to identify the frames that have to be decoded.

#234700 - $15.00 USD Received 13 Feb 2015; revised 20 Mar 2015; accepted 29 Mar 2015; published 10 Apr 2015

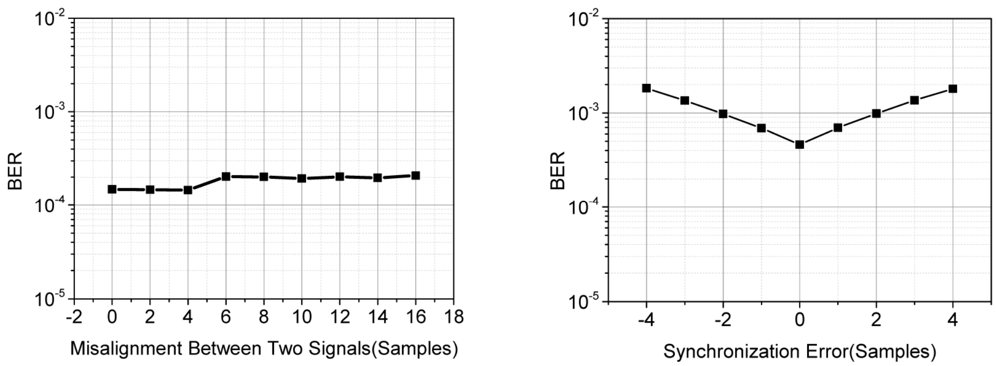

(a) (b)

Fig. 5. Simulation results: (a) BER performance under different misalignment between the two signals, represented by the number of samples, (b) BER performance under different synchronization error of the decoded arm between two signals.

4. Summary

We have experimentally demonstrated and characterized the application of OPNC in a CO-OFDM system. Individual OFDM frames are successfully separated and decoded at the destined receiver after the two source OFDM frames are optically combined in the immediate node. In the experiment, the OPNC achieved acceptable OSNR penalty and showed good feasibility of OPNC in coherent optical OFDM systems. This work was partially supported by a research grant from Hong Kong Research Grants Council (Project No. 14200614).

#234700 - $15.00 USD Received 13 Feb 2015; revised 20 Mar 2015; accepted 29 Mar 2015; published 10 Apr 2015